ACS APPLIED MATERIALS & INTERFACES

Research Article

www.acsami.org

Ultrasmall TiO_2 Nanoparticles in Situ Growth on Graphene Hybrid as Superior Anode Material for Sodium/Lithium Ion Batteries

Huiqiao Liu,‡ Kangzhe Cao,‡ Xiaohong Xu, Lifang Jiao,* Yijing Wang, and Huatang Yuan

Institute of New Energy Material Chemistry, Collaborative Innovation Center of Chemical Science and Engineering (Tianjin), Key Laboratory of Advanced Energy Materials Chemistry (MOE), Tianjin Key Lab of Metal and Molecule-based Material Chemistry, Nankai University, Tianjin 300071, People's Republic of China

Supporting Information

ABSTRACT: To inhibit the aggregation of TiO_2 nanoparticles and to improve the electrochemical kinetics of TiO_2 electrode, a hybrid material of ultrasmall TiO_2 nanoparticles in situ grown on rGO nanosheets was obtained by ultraphonic and reflux methods. The size of the TiO_2 particles was controlled about 10 nm, and these particles were evenly distributed across the rGO nanosheets. When used for the anode of a sodium ion battery, the electrochemical performance of this hybrid TiO_2@rGO was much improved. A capacity of 186.6 mAh g^{-1} was obtained after 100 cycles at 0.1 A g^{-1}, and 112.2 mAh g^{-1} could be maintained at 1.0 A g^{-1}, showing a high capacity and good rate capability. On the basis of the analysis of cyclic voltammetry (CV) and electrochemical impedance spectroscopy (EIS), the achieved excellent electrochemical performance was mainly attributed to the synergetic effect of well-dispersed ultrasmall TiO_2 nanoparticles and conductive graphene network and the improved electrochemical kinetics. The superior electrochemical performance of this hybrid material on lithium storage further confirmed the positive effect of rGO.

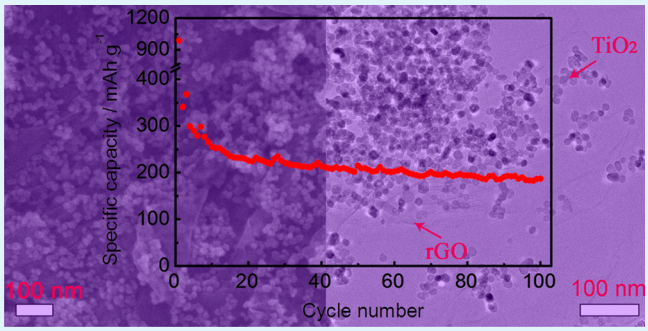

KEYWORDS: *ultrasmall TiO_2 nanoparticles, hybrid material, improved electrochemical kinetics, anode, Na^+ ion battery*

1. INTRODUCTION

As a multifunctional material, TiO_2 has been proven to have excellent performances in solar cell,[1,2] catalyst,[3] and hydrogen storage.[4,5] Meanwhile, it has been extensively researched when used as anode material for lithium ion batteries (LIBs). The advantages including nontoxic, abundant sources and structural stability during lithium insertion/extraction make TiO_2 to be an alternative material of LIBs anode.[6,7] However, because of the low lithium reserves and high cost of lithium, developing new batteries, such as sodium ion batteries (SIBs), becomes a research focus currently. As an abundant alkali element widely distributed around the world, sodium would be an ideal transporting ion for alternative rechargeable batteries. Furthermore, performances of TiO_2 used as anodes for SIBs have been substantiated by several pioneers' work because its 3D open structure could offer possible sites for Na location and proper sized pathways for Na diffusion. The redox of Ti^{4+}/Ti^{3+} is believed to be responsible for the capacity during sodium insertion−extraction, which is similar to the mechanism for LIBs.[8−11] However, because the size of Na^+ ions is larger than that of Li^+ ions, a sluggish kinetics because of the host electrode materials was required to have sufficiently larger interstitial space to accommodate sodium ions and to allow reversible and rapid ions/electrons insertion and extraction.[12] Meanwhile, the low conductivity of pure TiO_2 exacerbated the inferior electrochemical performance on Na^+ storage. Thus, the capacity and rate capability are not satisfied presently. Therefore, it is an urgent task to enhance the sluggish kinetics of Na^+ ion in TiO_2 to gain high capacity and good rate capability.

A usual and important strategy to enhance kinetics is to fabricate nanostructure materials, which has been widely adopted owing to its many merits.[13−16] Briefly speaking, a nanostructure electrode with a short ions diffusion path could largely enhance the electrochemical activity, and the enlarged electrode/electrolyte contact area is good for the ion loading; these are beneficial for high sodium/lithium storage and rate capability. What is more, the strain could be significantly reduced during charge and discharge processes, thus keeping the structural integrity of the electrode and leading to a stable cycle performance. However, nanoparticles tend to agglomerate during cycling because of the large surface energy; therefore, it is necessary to adopt some methods to prevent the agglomeration of nanoparticles.

Another strategy to enhance the kinetics is to improve the conductivity of TiO_2 by a doping modification, coating conductive and stable materials as well as hybridization with carbon materials, such as amorphous carbon,[17,18] carbon nanotubes,[16,19] and reduced graphene oxide nanosheet

Received: February 6, 2015
Accepted: May 12, 2015
Published: May 12, 2015

 © 2015 American Chemical Society

DOI: 10.1021/acsami.5b02724
ACS Appl. Mater. Interfaces 2015, 7, 11239−11245

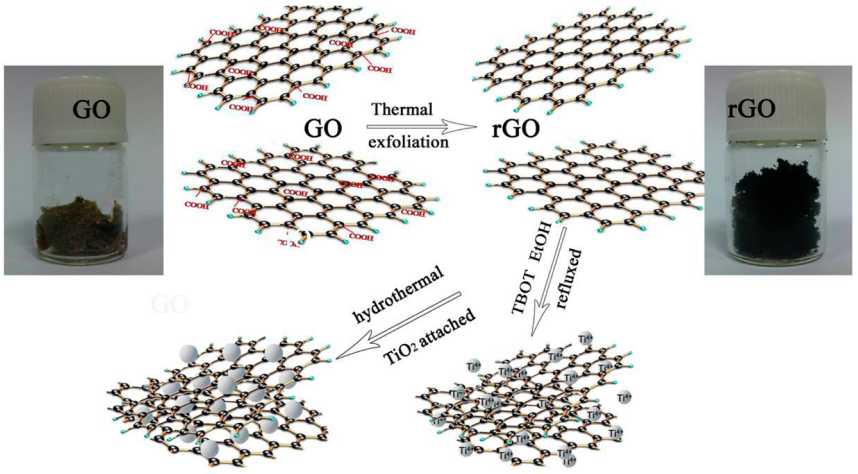

Figure 1. Illustration of the reduction of GO to rGO and ultrasmall TiO_2 nanoparticles attached on rGO.

(rGO).[20−22] Of these, rGO with its high conductivity, high specific surface area, significant thermodynamics, and chemical stability has caught more and more attention and has widely been used to construct hybrid materials.[23,24] When the rGO is used as a substrate for nanoparticles to scatter, the conductivity of the hybrid TiO_2 and rGO material is much improved, and the aggregation of the nanoparticles is effectively inhibited. However, according to the literature,[3,14,25] the TiO_2 particle sizes are not small enough (mostly larger than 20 nm), and the dispersions of the particles are not satisfied currently. Therefore, it would be better if the particle size could be further reduced and accompanied a satisfy dispersions.

In this work, rGO was adopted as a substrate for anchoring well-dispersed TiO_2 nanoparticles, and it worked as a highly conductive matrix. Combining ultrasonication and reflux, ultrasmall TiO_2 nanoparticles ca. 10 nm in situ grown on the surface of rGO were obtained. The large surface area of graphene made TiO_2 nanoparticles well dispersed, and the high homodispersed TiO_2 nanoparticles separated the reduced graphene oxide sheets reversely, preventing them from restacking. Because of the synergic effect of TiO_2 and rGO, the kinetics of this hybrid material electrode was enhanced, and it exhibited high capacity and excellent rate capability in sodium and lithium ion batteries.

2. EXPERIMENTAL SECTION

All the reagents were used as received without further purification.

2.1. Synthesis of rGO and Hybrid TiO_2@rGO. GO was synthesized from the chemical oxidation of graphite flakes by a modified Hummers method.[26] The as-prepared GO was then reduced by thermal exfoliation at a heating rate of 10 °C/min to 800 °C and was maintained for 1 min in a quartz tube under Ar−H_2 (9:1 in volume) flow to form rGO.

Typically, 30 mg rGO was dispersed in 100 mL ethanol with ultrasonication for 2 h, followed by adding 50 mL ethanol solution containing 0.5 g tetrabutyl titanate (TBOT). The mixture was heated to 80 °C and was refluxed for 3 h. Then, the well-mixed solution of 10 mL H_2O, 0.3 mL H_2SO_4, and 20 mL ethanol was added dropwise slowly to the above liquid, and it continued to reflux for 12 h. The obtained black solid was centrifuged and was washed with water and ethanol several times. The nanocomposite was dispersed into a mixed water/DMF solvent (50 mL/1 mL) and then was transferred into a 100 mL Teflon-lined stainless steel autoclave and was maintained at 200 °C for 12 h for a hydrothermal reaction. After separation and washing, the resultant composite was dried in a vacuum oven at 60 °C overnight.

2.2. Characterization. *2.2.1. Characterization of the As-Prepared Hybrid TiO_2@rGO.* The crystallinity and phase purity of hybrid TiO_2@rGO were examined using X-ray powder diffraction (XRD, Rigaku D/Max-2500, Cu Kα radiation). The XRD pattern was recorded from 3° to 80° (2θ) with a scanning speed of 4° per minute. The size and morphology of the resulting products were studied by scanning electron microscopy (SEM, Hitachi X-650). A Tecnai 20 transmission electron microscopy (TEM) was used for characterizing the inner structure of the materials. Raman spectra were recorded on Renishaw inVia with excitation of 514.5 nm. Nitrogen adsorption and desorption isotherms were detected by NOVA 2200e (quantachrome, USA). Thermogravimetric (TG) analysis of the hybrids was investigated on a TG-DTA (SETARAM S60) thermal analysis apparatus.

2.2.2. Electrochemical Measurements. The electrochemical performance of the materials was assessed by acting as anodes of sodium/lithium ion batteries. To prepare the working electrode, the slurry was prepared by intensively mixing 80 wt % hybrid TiO_2@rGO, 10 wt % Super-P carbon, and 10 wt % binder (polyvinylidene fluoride, PVDF) in *N*-methylpyrrolidinone (NMP) solvent. For comparison, a mixture of TiO_2 and rGO (22.5 wt %, named as mixture of TiO_2 + rGO) and pure TiO_2 were used as active materials to prepare control electrodes. The thick and uniform slurry of the mixture was smeared on copper foil with a diameter of 1 cm. The solvent was then evaporated by drying at 80 °C in a vacuum oven overnight. The electrochemical tests were carried out on two-electrode cells assembled in an argon-filled glovebox (O_2 < 1.0 ppm, H_2O < 1.0 ppm). For SIBs, sodium foil was used as the counter electrode, and glass fiber and 1 M $NaPF_6$ in polycarbonate (PC) and in fluoroethylene carbonate (FEC) (PC:FEC = 95:5, in volume) were separator and electrolyte. In terms of LIBs, the lithium metal was adopted as the counter electrode, and the electrolyte was 1 M $LiPF_6$ dissolved in an ethylene carbonate (EC)/dimethyl carbonate (DMC)/diethyl carbonate (DEC) mixture (EC:DMC:DEC = 1:1:1, in volume). The charge/discharge cycling was performed within the voltage range of 0.01−3 V versus Na^+/Na and Li^+/Li on a Land Battery Measurement system (Land CT2001A, Wuhan, China) at

DOI: 10.1021/acsami.5b02724
ACS Appl. Mater. Interfaces 2015, 7, 11239−11245

ambient temperature. Cyclic voltammogram (CV) and electrochemical impedance spectroscopy (EIS) were recorded using a CHI660b electrochemical working station (Chenhua, Shanghai, China).

3. RESULTS AND DISCUSSION

3.1. Characterization of rGO and Hybrid TiO_2@rGO. As illustrated in Figure 1, graphene oxide (GO) was obtained by a modified Hummers method[26] and appears as a yellow-brown color with a sheetlike appearance with naked eyes. After thermal exfoliation at high temperature (800 °C), the color became black and turned fluffy, suggesting the GO had been well reduced to rGO nanosheets. After these rGO nanosheets were thoroughly dispersed in the ethanol by ultrasonication, the tetrabutyl titanate was added and reflexed. In this process, the titanium precursor may firmly attach to the rGO nanosheets. When H_2O and H_2SO_4 are added, slow hydrolysis of the attached titanium precursor can lead to the in-situ formation of low-crystallization TiO_2 (Figure S1 of the Supporting Information). After a hydrothermal reaction, high crystallization ultrasmall TiO_2 nanoparticles attached on rGO.

Owing to the superior character of rGO, the quality of reduction from GO was characterized by XRD and Raman spectrum. The XRD patterns of GO in Figure 2a showed a strong peak at 11°, indicating the existence of a layered GO phase. The sharp peak was replaced by a broadened diffraction peak around 25° after the thermal treatment, confirming that GO had been well reduced to rGO nanosheets.[26] It was further proven by the Raman spectrum in Figure 2b. The D peak could be attributed to the creation of defect sites during thermal exfoliation, and the G peak could be assigned to sp^2 hybridized carbon. The intensity ratio of the I_D/I_G for rGO exhibits an enhanced value when compared with that of GO, suggesting the decrease of the oxygen-functional groups on GO.[28]

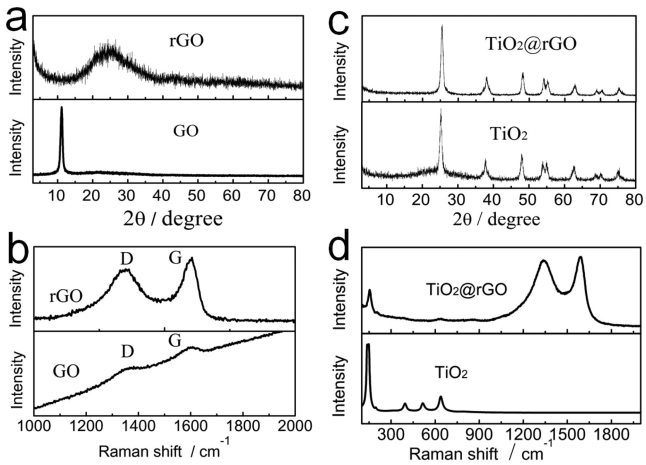

Figure 2. (a, c) XRD patterns and (b, d) Raman spectra of GO, rGO, TiO_2, and hybrid TiO_2@rGO.

The in situ formed hybrid TiO_2@rGO was also investigated by XRD and Raman spectrum. As shown in Figure 2c, the XRD pattern of the in situ formed hybrid TiO_2@rGO could be indexed to a typical anatase TiO_2 structure with space group $I4_1/amd$ (JCPDS card no. 21-1272). The diffraction peak of rGO disappeared in hybrid TiO_2@rGO. It is possible because the attachment of TiO_2 nanoparticles prevents them from restacking and destroys the ordered structure.[29] Compared with the XRD pattern of pure TiO_2, the diffraction peaks of hybrid TiO_2@rGO shifted slightly, indicating small crystal sized TiO_2 was obtained. Figure 2d shows the Raman spectra of the as-prepared pure TiO_2 as well as of the hybrid TiO_2@rGO. For pure TiO_2, a sharp Raman scattering peak was observed at 143 cm^{-1} because of E_g vibration modes of anatase, and the peaks at 400, 516, and 639 cm^{-1} corresponded to the different vibration modes of anatase. The Raman scattering peak at 152 cm^{-1} besides the two peaks (D band and G band) derived from rGO in the hybrid TiO_2@rGO was also observed. The blue shift in TiO_2 for hybrid TiO_2@rGO suggested a strong interaction between rGO nanosheets and individual TiO_2 particles.[27]

The morphologies and structures of rGO, pure TiO_2, and hybrid TiO_2@rGO were characterized by field emission scanning electron microscopy (SEM) and transmission electron microscopy (TEM). As depicted by Figure 3a, the rGO nanosheets still tended to be a slightly agglomerate state after thermal exfoliation, though largely enhanced compared to the GO (Figure S2 of the Supporting Information). Figure 3b shows the morphology of pure TiO_2. It can be seen clearly that a large part of TiO_2 nanoparticles aggregated together and that the particles appeared to vary in size ranging from 20 to 100 nm. In terms of the in situ formed hybrid TiO_2@rGO, the TiO_2 particles were closely anchored onto the surface of rGO and appeared as a homodispersion, making TiO_2 a larger specific area and fully in contact with the electrolyte when used as

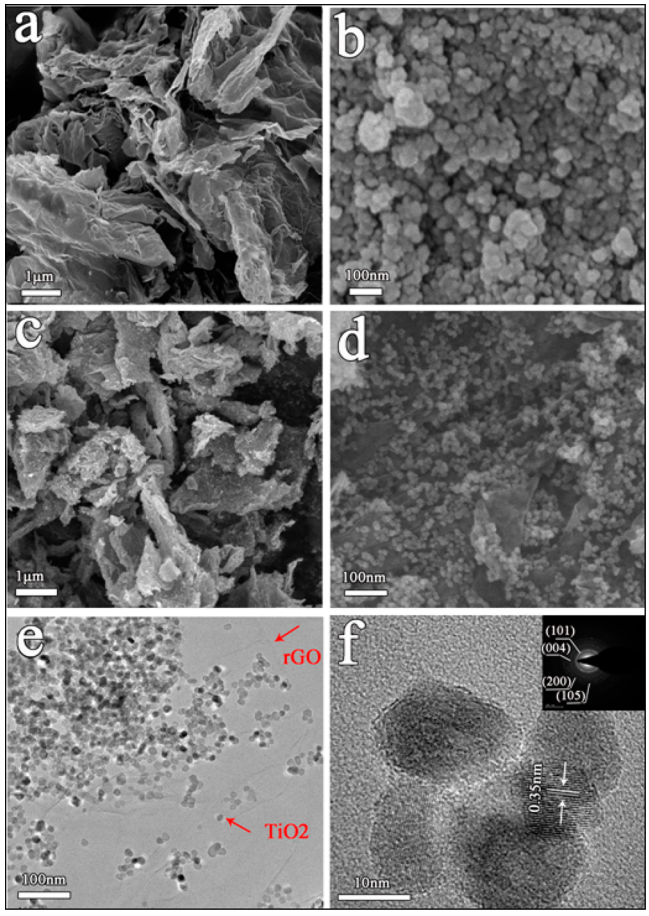

Figure 3. SEM images of (a) rGO and (b) as-prepared pure TiO_2; (c, d) SEM images and (e, f) TEM images and SAED pattern (inset of 3f) of hybrid TiO_2@rGO.

DOI: 10.1021/acsami.5b02724
ACS Appl. Mater. Interfaces 2015, 7, 11239−11245

anode materials of sodium and lithium ion batteries. Also, the restacking of rGO sheets may have received a certain degree of inhibition owing to the TiO_2 attachment. It was very important that most of the rGO sheets were covered by the TiO_2 nanoparticles and that the majority of the TiO_2 particles were anchored on the rGO sheets to ensure the efficient electron transfer via the rGO sheets during the insertion/extraction process.[30] TEM was used to further analyze the TiO_2 crystals on rGO nanosheets. The sizes of TiO_2 particles were around 10 nm and were well dispersed on the surface of rGO nanosheets. The high-resolution transmission electron microscopy (HR-TEM) images (Figure 3f) clearly showed the lattice fringe with a *d*-spacing of 0.35 nm, corresponding to (101) lattice plane of TiO_2. The insert picture of Figure 3f showed the selected-area electron diffraction (SAED) pattern of the TiO_2@rGO sample, with diffraction rings (101), (004), (200), and (105) of TiO_2, consistent with the XRD pattern in Figure 2c.[14]

The results of nitrogen adsorption−desorption experiments confirmed that the ultrasmall TiO_2 prepared by dispersing over rGO substrates had a larger specific surface area compared with pure TiO_2 in absence of rGO. As shown in Figure 4a, these

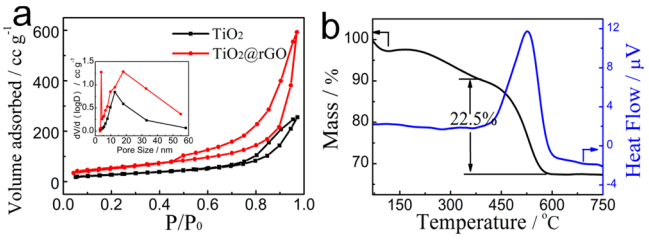

Figure 4. (a) N_2 adsorption and desorption isotherms and pore size distribution (insert) of as-prepared TiO_2 and hybrid TiO_2@rGO and (b) TG-DSC profiles of hybrid TiO_2@rGO.

nitrogen adsorption−desorption isotherms exhibited large distinct hysteresis loops which could be attributed to type IV.[31,32] As summarized in Table 1, the Brunauer−Emmett−

Table 1. Summary of the BET Characteristics of As-Prepared TiO_2 and Hybrid TiO_2@rGO

sample	S_{BET} (m^2/g)	pore size (nm)	pore volume (m^3/g)
TiO_2	104.73	12.6	0.401
Hybrid TiO_2@rGO	200.54	3.8 and 17.9	0.971

Teller (BET) surface area and the Barrett−Joyner−Halenda (BJH) pore volume of TiO_2 were significantly increased after the incorporation of rGO, ranging from 104.7 to 200.5 m^2 g^{-1} and from 0.401 to 0.971 cm^3 g^{-1}, respectively. It was noticeable that the pore size distribution had undergone great changes comparing pure TiO_2 and hybrid TiO_2@rGO. The BJH pore size distribution of TiO_2 was 12.6 nm, while it distributed within the two sizes of 3.8 and 17.9 nm when the TiO_2 particles decorated the surface of rGO sheets. The appearing of the 3.8 nm pore size was caused partly by the stacking reduced graphene and partly by the pore size among TiO_2 particles. The enlarged TiO_2 pore size also implied that these nanoparticles existed at a more homogeneous dispersion state when coated on rGO. The relatively large surface area and less aggregation of hybrid TiO_2@rGO would increase the electrolyte/electrode contact area, leading to a decrease of the current density per unit surface area and an increase in the charge/discharge rate.[16]

To measure the amount of rGO in the hybrid TiO_2@rGO, thermal studies were performed in air atmosphere at a heating rate of 10 °C/min. An exothermic peak at 380∼580 °C in the DSC curve was detected in Figure 4b, coinciding with 22.5% mass loss during the above heating temperature range. These features corresponded to the decomposition of rGO, so we could figure out that it contained 22.5 wt % of rGO in hybrid TiO_2@rGO, and the result (Table S1 of the Supporting Information) of elemental analyses (EA) also confirmed this result.

3.2. Electrochemical Performances. The electrochemical performance of hybrid TiO_2@rGO was first evaluated in sodium half-cells. Figure 5 shows the electrochemical perform-

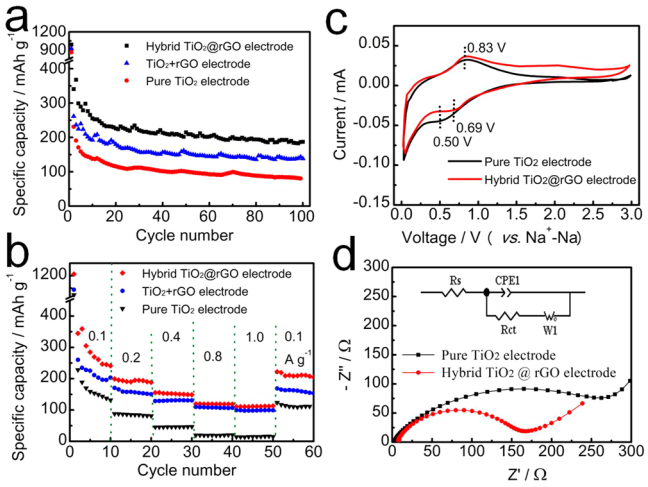

Figure 5. (a) The cycle performance at 0.1 Ag^{-1} and (b) the rate capabilities of hybrid TiO_2@rGO, a mixture of TiO_2 + rGO electrode, and pure TiO_2 (all the specific capacities is discharge capacities) for SIBs; (c) the third CV curves (0.2 mV s^{-1}) and (d) EIS (0.1−100k Hz) of pure TiO_2 electrode and hybrid TiO_2@rGO electrode for SIBs.

ances of hybrid TiO_2@rGO, a mixture of TiO_2 + rGO, and pure TiO_2 when used as the anode of SIBs. As revealed by the cycling performances, discharge capacities for the hybrid TiO_2@rGO, a mixture of TiO_2 + rGO, and pure TiO_2 electrodes at a current density of 0.1 A g^{-1} after 100 cycles were 186.6, 143.3, and 80.6 mAh g^{-1}, respectively. The capability of the hybrid TiO_2@rGO delivered was 2.3 times that of pure TiO_2 electrode and 1.3 times that of the mixture of TiO_2 + rGO. Obviously, the hybrid TiO_2@rGO electrode showed the best capacity and stability, while the pure TiO_2 electrode delivered the worst performance among the three electrodes. Meanwhile, the rate capabilities of the three electrodes duplicated the tendency of the cycling performance, and the hybrid TiO_2@rGO electrode displayed the best rate capability. As presented in Figure 5b, the average charge capacities of the hybrid TiO_2@rGO were 241, 190.3, 149.4, 118.7, and 112.2 mAh g^{-1} (the 10th cycle discharge capacity), respectively, at the different current densities of 0.1, 0.2, 0.4, 0.8, and 1.0 A g^{-1}. When the current density was finally directly reduced again to 0.1 A g^{-1}, the average capacity could recover to 222.3 mAh g^{-1}, showing an excellent rate capability. However, the pure TiO_2 electrode stayed at the capacities of 19.8 and 15.1 mAh g^{-1} when the current density increased to 0.8 and 1.0 Ag^{-1}. Although the capacity of TiO_2 could recover to 117.4 mAh g^{-1} when the current density returned to 0.1 Ag^{-1}, the weak performance of TiO_2 at high current densities

DOI: 10.1021/acsami.5b02724
ACS Appl. Mater. Interfaces 2015, 7, 11239−11245

showed an inferior rate capability. The mixture of TiO_2 + rGO electrode showed a comparable capacity to that of the hybrid TiO_2@rGO at high current densities. This result suggests that rGO plays a vital role in electron transfer at high current density, and the addition of rGO is important for enhancing the rate capability of the electrode.

Compared with the electrochemical performance of the three electrodes, the superior merits of the hybrid electrode could be studied when considering the cycling performance and the rate capability. In terms of hybrid TiO_2@rGO electrode and pure TiO_2 electrode, the addition of rGO largely expanded the specific surface of the TiO_2 by reducing the nanoparticle size and by avoiding the aggregation. When used as an electrode, rGO not only served as a part of the active material attributing to the capacity but also played the role of conductive network to transfer electrons during charge and discharge.[33] Also, the rGO acted as the substrate to prevent the TiO_2 nanoparticles from aggregating during cycling. Meanwhile, the adherence of TiO_2 on rGO effectively reduced the restacking of rGO sheets, which kept the hybrid material with a large surface during the charge and discharge cycles. The large surface with abundant active sites offered enough room for the Na^+ to locate, exhibiting a large capacity. However, the pure TiO_2 with smaller surface could not effectively transfer electrons especially at high current densities owing to its low conductivity; thus, a large polarization could not be avoided and bad aggregation happened, showing a lower capacity and inferior rate capability. When it came to the hybrid TiO_2@rGO electrode and mixture of TiO_2 + rGO electrode, the in-situ synthesis method made the TiO_2 and rGO mix thoroughly and attach to each other firmly because of the intermolecular force. On the contrary, the direct mixture of TiO_2 and rGO could not ensure a thorough mixture, which still reserved the aggregation of the TiO_2, and the restack of rGO nanosheets could not be avoided; thus, an unsatisfying performance could be predicted. However, a relatively better performance of the mixture of TiO_2 + rGO was obtained when compared with that of pure TiO_2 electrode, which illustrated the positive effect of rGO on the performance of electrodes and the necessity of the rGO addition.

The SEM images of the pure TiO_2 electrode (Figure S3a and d of the Supporting Information (SI)), mixture of TiO_2 + rGO electrode (Figure S3b and S3e of the SI), and hybrid TiO_2@rGO electrode (Figure S3c and S3f of the SI) after 100 charge and discharge cycles are provided in Figure S3 of the SI. Compared to the bad aggregation of pure TiO_2 electrode, the addition of rGO protects the TiO_2 nanoparticles from aggregating no matter in a directly mixed method or an in-situ method. Furthermore, the morphology of in situ formed hybrid TiO_2@rGO almost keeps its original state, which gives direct proof of the positive effect of rGO on preventing the aggregation of the TiO_2 nanoparticles.

Cyclic voltammetry (CV) is always used for detecting the electrochemical mechanism of the electrode. To further illustrate the positive effect of the rGO addition, the hybrid TiO_2@rGO and pure TiO_2 electrodes were performed by CV. Aiming to avoid the disturbance of the solid electrolyte interphase (SEI) layer formation and the occurrence of other irreversible reactions, the third cycle of the CV curves was chosen to examine the mechanism. As Figure 5c shows, a pair of redox peaks located at 0.50 and 0.83 V with 0.33 V peak separation (ΔE_1) were detected in the pure TiO_2 electrode, which was ascribed to the Na^+ insertion and extraction reaction into the host structure coupled with $Ti^{4+}/^{3+}$redox reaction, which was in accordance with previous works.[9,10] In terms of the copartner electrode, this pair of reversible peaks was detected at 0.69 and 0.83 V, of which the peak separation (ΔE_2) was 0.14 V. The higher sodiation voltage (0.69 V) in hybrid TiO_2@rGO electrode than that of pure TiO_2 (0.50 V) and a smaller peak separation (ΔE_2 = 0.14 V < ΔE_1 = 0.33 V) both indicate that the Na^+ insertion and extraction was much easier in the hybrid electrode, probably because of the improved kinetics of the hybrid electrode.[24,34]

The electrochemical impedance spectra for the hybrid TiO_2@rGO electrode and the pure TiO_2 electrode over the frequency range from 100k Hz to 0.1 Hz was investigated. As shown in Figure 5d, each Nyquist plot comprises two parts including a depressed semicircle at high frequency and a linear Warburg part at a low frequency, and the electrochemical system is simply modeled by a Randles equivalent circuit (where the R_s is the electrolyte resistance, CPE1 is the double-layer capacitance, R_{ct} is the charge-transfer resistance, and W1 is the Warburg impedance).[35] The semicircle is attributed to the R_{ct} at the electrolyte/electrode interface, and the latter linear is attributed to the diffusion of the sodium ions in the bulk of the electrode. Obviously, the R_{ct} of hybrid electrode was much lower than that of pure TiO_2 electrode on the basis of the modified Randles equivalent circuit. Also, the exchange current densities (i^0) could be compared according to the equation ($i^0 = RT/nFR_{ct}$), which confirmed the improved kinetics.[35,36]

When this hybrid material was used as an LIB anode, a similar performance could be seen, as presented by Figure S4 of the SI. The capacity and rate capability of hybrid TiO_2@rGO electrode were better than that of pure TiO_2 electrode, and the CV curves and EIS also confirmed that the rGO provided a positive effect on the electrochemical performance of the electrode. To the best of our knowledge, the electrochemical performance of this hybrid TiO_2@rGO electrode is the best one among the reported TiO_2 based electrodes, no matter in SIBs or LIBs. The comparative results are listed in the Supporting Information, Table S2 (for SIBs) and Table S3 (for LIBs).

Though the capacity and rate capability of the TiO_2 are improved by adding rGO no matter in SIBs or LIBs, the side effect of the rGO on the electrode cannot be ignored. Considering that the rGO was prepared by the modified Hummers' method, amounts of impurities, hydrocarbons, and heteroatoms on the graphene surfaces may be unavoidably generated by the oxidative process in strong acid.[37] This is one reason for the low Coulombic efficiency (Figure S5 of the SI) during the initial cycles. Besides, the inevitable formation of SEI layer and decomposition of electrolyte also could lead to the irreversible capacity loss, resulting in a low Coulombic efficiency.[36,38]

4. CONCLUSIONS

In this paper, a hybrid TiO_2@rGO material was synthesized by an in-situ method. Because of the interaction between TiO_2 nanoparticles and the residual functional groups of rGO, the size of the TiO_2 was effectively controlled and the aggregation was perfectly prevented. When used as anode of SIBs, a capacity of 186.6 mAh g^{-1} was obtained after 100 cycles at 0.1 A g^{-1}. Even the current densities increased to 1.0 A g^{-1}, and a capacity of 112.2 mAh g^{-1} was still maintained, showing a good rate capability. An excellent electrochemical performance for Li storage was also obtained when this hybrid material was used as LIBs anode. The presented superior electrochemical perform-

DOI: 10.1021/acsami.5b02724
ACS Appl. Mater. Interfaces 2015, 7, 11239−11245

ance on SIBs and LIBs was because of the enhanced kinetics produced by the rGO addition and the synergetic effect between well-dispersed ultrasmall TiO_2 nanoparticles and conductive graphene network.

■ ASSOCIATED CONTENT

Supporting Information

Tables for the electrochemical performances on SIBs and LIBs of the hybrid TiO_2@rGO electrode and the relative reported works. The XRD patterns of hybrid TiO_2@rGO before hydrothermal reaction and rGO, SEM images of GO. The SEM images for the electrodes after 100 charge and discharge cycles for SIBs. The electrochemical performance of pure TiO_2 electrode and hybrid TiO_2@rGO electrode for LIBs, and the Coulombic efficiency of hybrid TiO_2@rGO electrode for SIBs and LIBs. The Supporting Information is available free of charge on the ACS Publications website at DOI: 10.1021/acsami.5b02724.

■ AUTHOR INFORMATION

Corresponding Author

*E-mail: jiaolf@nankai.edu.cn.

Author Contributions

‡These authors contributed equally.

Notes

The authors declare no competing financial interest.

■ ACKNOWLEDGMENTS

This work was financially supported by the National Natural Science Foundation of China (51231003), the Ministry of Education of China (IRT-13R30), and the 111 Project (B12015).

■ REFERENCES

(1) Zhu, K.; Neale, N. R.; Miedaner, A.; Frank, A. J. Enhanced Charge-collection Efficiencies and Light Scattering in Dye-sensitized Solar Cells Using Oriented TiO_2 Nanotubes Arrays. *Nano Lett.* **2007**, *7*, 69−74.

(2) Wang, X. Y.; Sun, L. D.; Zhang, S.; Wang, X. Ultra-long, Small-diameter TiO_2 Nanotubes Achieved by an Optimized Two-step Anodization for Efficient Dye-sensitized Solar Cells. *ACS Appl. Mater. Interfaces* **2014**, *6*, 1361−1365.

(3) Liang, Y. Y.; Wang, H. L.; Sanchez, C.; He, N.; Chen, Z.; Dai, H. J. TiO_2 Nanocrystals Grown on Graphene as Advanced Photocatalytic Hybrid Materials. *Nano Res.* **2010**, *3*, 701−705.

(4) Liu, H. Q.; Jiao, L. F.; Zhao, Y. P.; Cao, K. Z.; Liu, Y. C.; Wang, Y. J.; Yuan, H. T. Improved Dehydrogenation Performance of $LiBH_4$ by Confinement into Porous TiO_2 Micro-tubes. *J. Mater. Chem. A* **2014**, *2*, 9244−9250.

(5) Kathryn, E. D.; Wang, C.; Lin, W. B. Metal-organic Framework Templated Synthesis of Fe_2O_3/TiO_2 Nanocomposite for Hydrogen Production. *Adv. Mater.* **2012**, *24*, 2014−2018.

(6) Han, H.; Song, T.; Lee, E. K.; Devadoss, A.; Jeon, Y.; Ha, J.; Chung, Y. C.; Choi, Y. M.; Jung, Y. G.; Paik, U. Dominant Factors Governing the Rate Capability of a TiO_2 Nanotube Anode for High Power Lithium Ion Batteries. *ACS Nano* **2012**, *6*, 8308−8315.

(7) Kim, G.; Jo, C. S.; Kim, W.; Chun, J. Y.; Yoon, S. H.; Lee, J. W.; Choi, W. Y. TiO_2 Nanodisks Designed for Li-ion Batteries: a Novel Strategy for Obtaining an Ultrathin and High Surface Area Anode Material at the Ice Interface. *Energy Environ. Sci.* **2013**, *6*, 2932−2399.

(8) Xiong, H.; Slater, M. D.; Balasubramanian, M.; Johnson, C. S.; Rajh, T. Amorphous TiO_2 Nanotube Anode for Rechargeable Sodium Ion Batteries. *J. Phys. Chem. Lett.* **2011**, *2*, 2560−2565.

(9) Kim, K. T.; Ali, G.; Chung, K. Y.; Yoon, C. S.; Yashiro, H.; Sun, Y. K.; Lu, J.; Amine, K.; Myung, S. T. Anatase Titania Nanorods as an Intercalation Anode Material for Rechargeable Sodium Batteries. *Nano Lett.* **2014**, *14*, 416−422.

(10) Xu, Y.; Lotfabad, E. M.; Wang, H. L.; Farbod, B.; Xu, Z. W.; Kohandehghan, A.; Mitlin, D. Nanocrystalline Anatase TiO_2: a New Anode Material for Rechargeable Sodium Ion Batteries. *Chem. Commun.* **2013**, *49*, 8973−8975.

(11) Huang, J. P.; Yuan, D. D.; Zhang, H. Z.; Cao, Y. L.; Li, G. R.; Yang, H. X.; Gao, X. P. Electrochemical Sodium Storage of TiO_2(B) Nanotubes for Sodium Ion Batteries. *RSC Adv.* **2013**, *3*, 12593−12597.

(12) Dahbi, M.; Yabuuchi, N.; Kubota, K.; Tokiwac, K.; Komaba, S. Negative Electrodes for Na-ion Batteries. *Phys. Chem. Chem. Phys.* **2014**, *16*, 15007−15028.

(13) He, M.; Kravchyk, K.; Walter, M.; Kovalenko, M. V. Monodisperse Antimony Nanocrystals for High-rate Li-ion and Na-ion Battery Anodes: Nano versus Bulk. *Nano Lett.* **2014**, *14*, 1255−1262.

(14) Saravanan, K.; Ananthanarayanan, K.; Balaya, P. Mesoporous TiO_2 with High Packing Density for Superior Lithium Storage. *Energy Environ. Sci.* **2010**, *3*, 939−948.

(15) Rai, A. K.; Anh, L. T.; Gim, J.; Mathew, V.; Kang, J.; Paul, B. J.; Song, J. J.; Kim, J. Simple Synthesis and Particle Size Effects of TiO_2 Nanoparticle Anodes for Rechargeable Lithium Ion Batteries. *Electrochim. Acta* **2013**, *90*, 112−118.

(16) Shen, L. F.; Zhang, X. G.; Li, H. S.; Yuan, C. Z.; Cao, G. Z. Design and Tailoring of a Three-dimensional TiO_2−graphene−carbon Nanotube Nanocomposite for Fast Lithium Storage. *J. Phys. Chem. Lett.* **2011**, *2*, 3096−3101.

(17) Wang, W. S.; Sa, Q. N.; Chen, J. H.; Wang, Y.; Jung, H.; Yin, Y. D. Porous TiO_2/C Nanocomposite Shells As a High-performance Anode Material for Lithium-ion Batteries. *ACS Appl. Mater. Interfaces* **2013**, *5*, 6478−6483.

(18) Ryu, M. H.; Jung, K. N.; Shin, K. H.; Han, K. S.; Yoon, S. High Performance N-doped Mesoporous Carbon Decorated TiO_2 Nanofibers as Anode Materials for Lithium-Ion Batteries. *J. Phys. Chem. C* **2013**, *117*, 8092−8098.

(19) Nguyen, J.; Holland, T. B.; Wen, H.; Fraga, M.; Mukherjee, A.; Lavernia, E. Mechanical Behavior of Ultrafine-grained Ni−carbon Nanotube Composite. *J. Mater. Sci.* **2014**, *49*, 2070−2077.

(20) Zhang, X.; Kumar, P. S.; Aravindan, V.; Liu, H. H.; Sundaramurthy, J.; Mhaisalkar, S. G.; Duong, H. M.; Ramakrishna, S.; Madhavi, S. Electrospun TiO_2−graphene Composite Nanofibers as a Highly Durable Insertion Anode for Lithium Ion Batteries. *J. Phys. Chem. C* **2012**, *116*, 14780−14788.

(21) Wang, D. H.; Choi, D.; Li, J.; Yang, Z. G.; Zhang, J. G.; Nie, Z. M.; Kou, R.; Hu, D. G.; Wang, C. M.; Saraf, L. V.; Zhang, G. J.; Aksay, I. A.; Liu, J. Self-assembled TiO_2−graphene Hybrid Nanostructures for Enhanced Li-ion Insertion. *ACS Nano* **2009**, *3*, 907−914.

(22) Qiu, Y. C.; Yan, K. Y.; Yang, S. H.; Jin, L. M.; Deng, H. Synthesis of Size-tunable Anatase TiO_2 Nanospindles and Their Assembly into Anatase@Titanium Oxynitride/Titanium Nitride Graphene Nanocomposites for Rechargeable Lithium Ion Batteries with High Cycling Performance. *ACS Nano* **2010**, *4*, 6515−6526.

(23) Zhang, M.; Huang, L.; Chen, J.; Li, C.; Shi, G. Q. Ultratough, Ultrastrong, and Highly Conductive Graphene Films with Arbitrary Sizes. *Adv. Mater.* **2014**, *26*, 7588−7592.

(24) Mai, Y. J.; Zhang, D.; Qiao, Y. Q.; Gu, C. D.; Wang, X. L.; Tu, J. P. MnO/reduced Graphene Oxide Sheet Hybrid as an Anode for Li-ion Batteries with Enhanced Lithium Storage Performance. *J. Power Sources* **2012**, *216*, 201−207.

(25) Cha, H. A.; Jeong, H. M.; Kang, J. K. Nitrogen-doped Open Pore Channeled Graphene Facilitating Electrochemical Performance of TiO_2 Nanoparticles as an Anode Material for Sodium Ion Batteries. *J. Mater. Chem. A* **2014**, *2*, 5182−5186.

(26) Kovtyukhova, N. I.; Ollivier, P. J.; Martin, B. R.; Mallouk, T. E.; Chizhik, S. A.; Buzaneva, E. V.; Gorchinskiy, A. D. Layer-by-layer Assembly of Ultrathin Composite Films from Micron-sized Graphite Oxide Sheets and Polycations. *Chem. Mater.* **1999**, *11*, 771−778.

DOI: 10.1021/acsami.5b02724
ACS Appl. Mater. Interfaces 2015, 7, 11239−11245

(27) Etacheri, V.; Yourey, J.; Bartlett, B. M. Chemically Bonded TiO_2–bronze Nanosheet/Reduced Graphene Oxide Hybrid for High-power Lithium Ion Batteries. *ACS Nano* **2014**, *8*, 1491–1499.
(28) Liu, G.; Wang, Y. J.; Xu, C. C.; Qiu, F. Y.; An, C. H.; Li, L.; Jiao, L. F.; Yuan, H. T. Excellent Catalytic Effects of Highly Crumpled Graphene Nanosheets on Hydrogenation/Dehydrogenation of Magnesium Hydride. *Nanoscale* **2013**, *5*, 1074–1081.
(29) Li, D.; Shi, D. Q.; Liu, Z. W.; Liu, H. K.; Guo, Z. P. TiO_2 Nanoparticles on Nitrogen-doped Graphene as Anode Material for Lithium Ion Batteries. *J. Nanopart. Res.* **2013**, *15*, 1674–1683.
(30) Qiu, J.; Zhang, P.; Ling, M.; Li, S.; Liu, P.; Zhao, H.; Zhang, S. Photocatalytic Synthesis of TiO_2 and Reduced Graphene Oxide Nanocomposite for Lithium Ion Battery. *ACS Appl. Mater. Interfaces* **2012**, *4*, 3636–3642.
(31) Du, H. M.; Jiao, L. F.; Cao, K. Z.; Wang, Y. J.; Yuan, H. T. Polyol-mediated Synthesis of Mesoporous α-$Ni(OH)_2$ with Enhanced Supercapacitance. *ACS Appl. Mater. Interfaces* **2013**, *5*, 6643–6648.
(32) Luo, W.; Hu, X. L.; Sun, Y. M.; Huang, Y. H. Controlled Synthesis of Mesoporous MnO/C Networks by Microwave Irradiation and Their Enhanced Lithium-storage Properties. *ACS Appl. Mater. Interfaces* **2013**, *5*, 1997–2003.
(33) Gao, G. X.; Wu, H. B.; Lou, X. W. Citrate-assisted Growth of $NiCo_2O_4$ Nanosheets on Reduced Graphene Oxide for Highly Reversible Lithium Storage. *Adv. Energy Mater.* **2014**, *4*, 1400422.
(34) Sun, Y. M.; Hu, X. L.; Luo, W.; Xia, F. F.; Huang, Y. H. Reconstruction of Conformal Nanoscale MnO on Graphene as a High-capacity and Long-life Anode Material for Lithium Ion Batteries. *Adv. Funct. Mater.* **2013**, *23*, 2436–2444.
(35) Shen, L. F.; Uchaker, E.; Zhang, X. G.; Cao, G. Z. Hydrogenated $Li_4Ti_5O_{12}$ Nanowire Arrays for High Rate Lithium Ion Batteries. *Adv. Mater.* **2012**, *24*, 6502–6506.
(36) Cao, K. Z.; Jiao, L. F.; Liu, H. Q.; Liu, Y. C.; Wang, Y. J.; Guo, Z. P.; Yuan, H. T. 3D Hierarchical Porous Fe_2O_3 Nanosheets for High-performance Lithium-ion Batteries. *Adv. Energy Mater.* **2015**, *5*, 1401421.
(37) Wang, Y. X.; Chou, S. L.; Liu, H. K.; Dou, S. X. Reduced Graphene Oxide with Superior Cycling Stability and Rate Capability for Sodium Storage. *Carbon* **2013**, *57*, 202–208.
(38) He, C. N.; Wu, S.; Zhao, N. Q.; Shi, C. S.; Liu, E. Z.; Li, J. J. Carbon-encapsulated Fe_3O_4 Nanoparticles as a High-rate Lithium Ion Battery Anode Material. *ACS Nano* **2013**, *7*, 4459–4469.

DOI: 10.1021/acsami.5b02724
ACS Appl. Mater. Interfaces 2015, 7, 11239–11245